



## The application of dither to mitigate curve squeal

Downloaded from: <https://research.chalmers.se>, 2022-01-01 18:15 UTC

Citation for the original published paper (version of record):

Kropp, W., Theyssen, J., Pieringer, A. (2021)  
The application of dither to mitigate curve squeal  
Journal of Sound and Vibration, 514  
<http://dx.doi.org/10.1016/j.jsv.2021.116433>

N.B. When citing this work, cite the original published paper.

Contents lists available at [ScienceDirect](https://www.sciencedirect.com)

## Journal of Sound and Vibration

journal homepage: [www.elsevier.com/locate/jsvi](http://www.elsevier.com/locate/jsvi)

## The application of dither to mitigate curve squeal

Wolfgang Kropp\*, Jannik Theyssen, Astrid Pieringer

Division of Applied Acoustics, Chalmers University of Technology, SE-41296 Göteborg, Sweden

## ARTICLE INFO

## Keywords:

Squealing noise  
Self-excited vibrations  
Railway noise  
Dither control

## ABSTRACT

Curve squeal is a highly disturbing tonal sound generated by rail vehicles like trains, metros or trams, when negotiating a sharp curve. The probability that squeal occurs increases with reduced curve radius of the track. Curve squeal noise is attributed to self-excited vibrations caused by stick/slip behaviour due to lateral creepage of the wheel tyre on the top of the rail. With respect to the large number of rolling stock units and the long lifetime of vehicles, there is an urgent need for a cheap and simple retrofitting measure to reduce curve squeal. Therefore, main objective of this paper is to investigate the potential to reduce curve squeal by means of active control in the form of dither in an efficient and robust way. Dither control has been applied in the field of mechanical engineering for systems including non-linear components. There it has been shown to suppress self-excited oscillations very efficiently. The control is an open-loop control. It consists in adding a forced vibration to the vibrational system. A time-domain model has been applied to investigate the mechanisms behind self-excited vibrations leading to curve squeal at the squealing noise rig at Chalmers University of Technology. The analysis showed, that in the presence of constant friction, the coupling between lateral and vertical direction is the driving mechanism for building up self-excited vibrations. Based on this insight, the potential of dither has been investigated. For the case considered here dither has the potential to reduce the overall kinetic energy on the wheel by more than 10 dB and on the rail by more than 20 dB. Further optimisation of dither forces with respect to the radiated sound power might increase this potential.

## 1. Background

Curve squeal is highly annoying due to its tonal character and its high amplitudes. It may be generated when rail vehicles negotiate tight curves. For curves with a radius of 200 m and below, curve squeal is common. At the same time, such tight curves occur mainly in urban areas where many people live close to the tracks. Therefore, curve squeal can contribute to the negative health impact of traffic noise. Curve squeal is also a comfort issue for passengers. In [1], it is stated that about 7 percent of railway customers are highly disturbed by curve squeal noise. Curve squeal noise is attributed to self-excited vibrations caused by stick/slip behaviour due to lateral creepage of the wheel tyre on the top of the rail [2]. However, the actual mechanism of the instability is still a controversial topic. It is either explained by a falling friction curve (see e.g. [3–5]) or by mode coupling between normal and lateral dynamics [6–8]. Recently, it was shown that instability can be observed for a constant friction curve even without mode coupling (e.g. [9,10]). For the reduction of curve squeal noise mainly three measures are available:

- There have been several attempts made to optimise the design of wheel and rail towards less curve squeal. Most successful seems to be the asymmetric rail profile [11] moving the contact position on the inner wheel outside the so-called “squeal zone”. There are, however, no implementations of improved design on the market.

\* Corresponding author.

E-mail address: [wolfgang.kropp@chalmers.se](mailto:wolfgang.kropp@chalmers.se) (W. Kropp).<https://doi.org/10.1016/j.jsv.2021.116433>

Received 22 March 2021; Received in revised form 27 August 2021; Accepted 31 August 2021

Available online 8 September 2021

0022-460X/© 2021 The Author(s). Published by Elsevier Ltd. This is an open access article under the CC BY license

<http://creativecommons.org/licenses/by/4.0/>.

- Lubrication of the rail with grease, water or specially developed friction modifiers has been shown to be efficient in some cases [12], while it failed in others [13]. By reducing the friction coefficient, curve squeal might be eliminated. Problems could be insufficient traction forces, soil contamination close to the track, or, when using pure water, the need to avoid freezing.
- Wheel dampers showed in some situations good results. By adding constrained damping layers [14] or so-called ring dampers [15], substantial reduction could be achieved if the damped modes were involved in the curve squeal. In this context, the amount of reduction is not proportional to the increase in damping. Already little additional damping can suppress the self-excitation of stick-slip motions and therefore give high reduction.

To conclude, it seems to be difficult to offer a sustainable and reliable solution to the problem of curve squeal. While new design does not solve the problems with existing infrastructure, wheel damping and lubrication have shown to work in certain situations, but to fail in others. With respect to the large number of the rolling stock units and the long lifetime of vehicles there is obviously an urgent need for a cheap and simple retrofitting measure to reduce curve squeal. An approach that recently has been suggested for the mitigation of squealing noise is the use of dither [16]. The application of dither means that an additional signal (the dither signal) is added to the vibrational system to suppress self-excited vibrations. The objective of this work is to increase the understanding of the mechanisms behind squeal and to further investigate the potential for reducing curve squeal based on the dither approach. Such an approach could also open for fast and cheap retrofitting both on track and wheel. The idea of dither as presented in literature is discussed in the next section followed by a brief description of the model used to investigate curve squeal and the functioning of dither, and a presentation of the test case used in this work in Section 3. Section 4 discusses in detail the mechanism behind the occurrence of curve squeal for the case considered here. Based on these insights, the functioning of dither to suppress curve squeal is investigated (see Section 5). The results are finally summarised in the Conclusions.

## 2. Dither signals to control self-excited vibrations

Typical examples of self-excited vibrations are combustion instabilities or friction oscillators. In a self-excited system non-oscillatory energy is transformed to oscillatory energy due to a feedback process. The vibrations are growing typically at a frequency close to eigenfrequencies of the involved systems. The rate of growth is often determined by the internal damping in the systems. The vibrations might reach a certain saturation level which is determined by the underlying physical processes. For instance, the vibrations of a friction oscillator come into a saturation state when the vibrations levels are high enough to approach the sticking zone on the friction curve. When discussing dither in this context, one may first think of active control, which has been shown to be suitable to disturb this feedback process and suppress the build-up process of the self-excited vibrations. Maria Heckl was probably the first who successfully has used this approach for the control of the noise generation from the Rijke tube [17]. Other examples concern unstable combustion [18], machine chatter using active bearings [19], or torsional vibrations in a drillstring [20]. Maria Heckl also used an active control approach for the control of curve squeal noise [21–23]. With a pre-calculated control law she fed back wheel vibrations to force transducers either on the wheel or the rail. She also demonstrated the functioning of the approach in a simplified experimental set-up.

In “standard” active control the original field is carefully observed (e.g. the vibration in reference positions) and an additional field is created by active sources and added to the field to change e.g. radiation or propagation properties. This approach demands high accuracy in amplitude and phase for the added field. For destroying the feedback process by active means, the required control laws are shown to be more relaxed. Both amplitude and phase have just to be in a certain range. This is the strength of the application of active control in the case of self-excited vibrations. In this aspect, dither goes even a step further as it is an open-loop approach that can work without observing the original field. It has been widely used in different areas such as audio recording techniques, optics, image processing, and control technology. The expression refers to the application of signals/information to a system in order to modify its characteristics. A specific example is the use of dither to compensate for the negative consequence of quantisation errors. By adding shaped noise to the audio signals before the digital/analog converting process the perceived audio quality is improved substantially (see e.g. [24] and [25]). Dither control also has been applied in the field of mechanical engineering. Especially for systems including non-linear components dither can be used to suppress self-excited oscillations. Morgül [26] showed that in the case of friction oscillators, dither control could be used to prevent the build-up of stick/slip motion. He investigated the control of chaotic systems with dither and showed that there are no restrictions with respect to frequency content or time behaviour of the dither signals other than that the frequency content has to be higher than the friction-induced response. As dither control is an open-loop control and is superposed to the existing field without any feedback, its implementation is simple and does not require any control environment as traditional active control approaches do. Up to now very little has been published on dither control of curve squeal as far as the authors can conclude from literature. Dither control of self-excited vibrations has mainly been investigated for generic cases such as simple oscillators with friction elements (see e.g. [27] and [28]). There, it was shown that dither control could be used to modify the effective friction characteristics. It also has been shown that the underlying friction characteristic is essential for the functioning of dither [28]. Besides for simple oscillators, dither control has also been used for the control of brake disc squeal in automotive applications. Cunefare [29] and later Bardetscher et al. [30] showed for disc brake rotor squeal that “normal dither” could be used to reduce and even suppress the generation of squeal. The performance of the brakes was only marginally reduced. “Normal dither” in this context means that the dither control changed the normal force between the brake pad and the brake disc. An alternative is “tangential dither”. There seems no general rule for selecting the signal form and amplitude, although e.g. in [31] it was shown that periodic square signals are much more effective than sinusoidal signals.

In [29] a harmonic signal was used as dither with a frequency above the eigenfrequencies of the squeal modes under consideration. Even frequencies outside the audible range (i.e. above about 20 kHz) were shown to work in this application. In

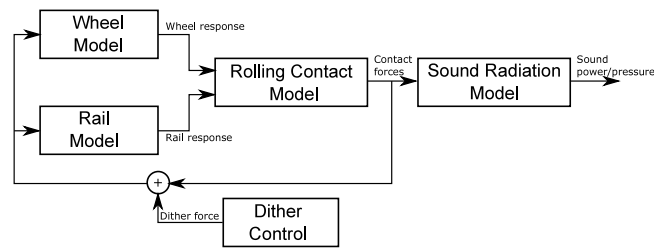


Fig. 1. Design of WERAN for the simulation of rolling and squeal noise generation in the contact between wheel and rail.

this case, the dither signal is not audible. Therefore, the control is not adding a disturbing tonal signal. The first application of dither to mitigate squeal noise from railway systems is presented in [16] for the case of a falling friction curve. A numerical model was used to demonstrate the function of dither when using a piezo stack at the wheel or the rail as excitation. The results were encouraging, although the mechanism behind the functioning of dither was not explained in detail.

### 3. Modelling curve squeal

To model the intrinsically non-linear and transient phenomenon of curve squeal is numerically challenging, just considering the complexity of the involved structures, the need to include non-linear transient rolling contact and the wide frequency range. While frequency domain models can be used to investigate which modes are prone to squeal, amplitudes of squeal can only be predicted by time domain models. However, modelling in the time domain increases the computational effort substantially. Consequently, many of the existing time domain models rely on simplifications of wheel, rail, or contact formulation. Typically, the track dynamics are neglected, and the consequences of this simplification are not clear. The few who include track dynamics (e.g. [32–35]) do not come to an agreement on this issue. However, we know from practice that changes in the track design can increase or decrease the problems with curve squeal [36]. Most models describe the relation between creep force and creep in a form, which can only partly represent the non-linear process in the contact zone. Périard [32], for instance, included a modified version of Kalker's steady-state contact model FASTSIM [37] in his squeal model. These simplifications, however, might be needed to reach a sufficient computational efficiency, allowing for e.g. extensive parameter studies.

#### 3.1. The curve squeal model at Chalmers, Applied Acoustics

In this paper a modified version of the WERAN (WhEel/RAil Noise) model is used. The original model has been developed by Pieringer [38]. She combined pre-calculated impulse response functions for track and wheel with the model by Kalker for transient rolling contact [39]. Track responses are calculated with Waveguide Finite Elements, while a standard Finite Element Model with axisymmetric elements is used for the wheel. In this way, the complete dynamics of wheel and track in the required frequency range is considered in combination with a fully three-dimensional transient and non-linear contact model. The computational costs are acceptable in contrast to the computational costs of an equivalent full Finite Element Model for curve squeal. However, the costs might still be too high for many engineering applications. Zenzerovic therefore developed an “engineering” version of the model by Pieringer [40,41].

The overall structure of the engineering version of WERAN (already with the addition of dither forces) is shown in Fig. 1. The required input to WERAN is as follows

- The assumed or pre-calculated creepage and contact position, based on vehicle dynamics simulations.
- The roughness of wheel and rail in several parallel tracks around the wheel and along the rail.
- The pre-calculated dynamic wheel and track response at the contact position given as Green's functions.
- The exact contact geometry and pre-load as input to the vertical contact model based on Kalker's variational theory [39].
- In the engineering version, the regularised friction curve for the fast tangential one point-contact formulation. This regularised friction curve is pre-calculated using Kalker's variational theory. The calculations are done for each set of contact parameters assuming Coulomb friction in each contact element.

In WERAN for each time-step, the wheel and track response are convolved to provide the displacements of both bodies as an input to the contact model. The normal contact problem is solved first, providing the normal load as an input to the lateral contact. The lateral problem is solved subsequently, and the vertical and longitudinal contact forces serve as inputs to the next convolution step of the dynamic wheel and track response.

In a post-processing step, the vibrations of the wheel and the track could be calculated as input to an in-house developed Boundary Element model to calculate sound radiation. For the work in this paper, however, this model is not utilised.

To include dither is straightforward in this modelling approach as it means just adding additional forces which are varying over time in a prescribed way as shown in Fig. 1.

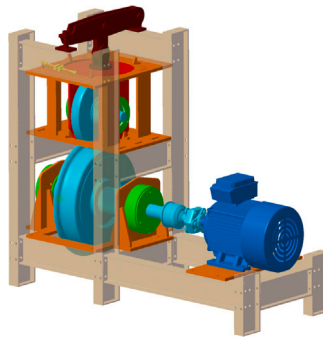


Fig. 2. Squealing noise rig at Applied Acoustics. Lower wheel driven by an engine. Upper wheel representing the rail.

**Table 1**  
Radius and modal damping ratio for wheel and rail.  $n$  indicates the number of wavelengths on the circumference.

	Radius in m	$\zeta_n$ for $n = 0$	$\zeta_n$ for $n = 1$	$\zeta_n$ for $n > 1$
Wheel	0.261	0.001	$n = 0.01$	0.0001
Rail	0.190	0.1	1	0.01

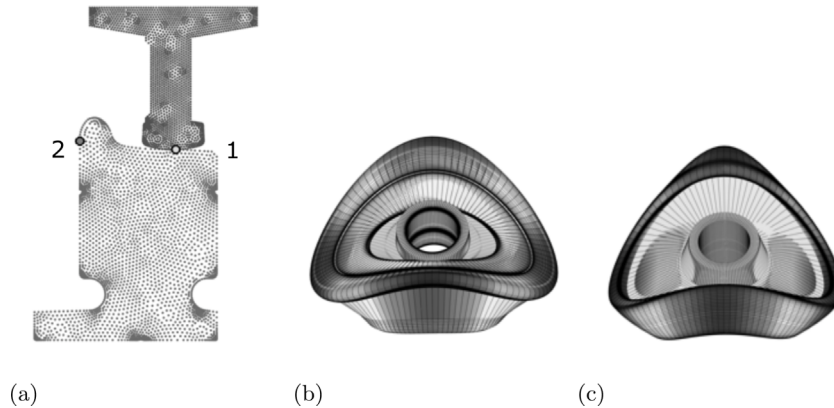


Fig. 3. (a) Cross-section of wheel and rail, contact position (position 1) and the position where dither is applied (position 2). (b) Mode shape for the mode (2,0,a) for the wheel (eigenfrequency 2008 Hz). (c) Mode shape for the mode (2,0,a) for the rail (eigenfrequency 2049 Hz).

### 3.2. Test setup

For investigating the dither approach, the model is adapted to the squeal noise rig (see Fig. 2) recently built at the division of Applied Acoustics [42].

The use of the squealing noise rig as a test object is motivated by the future plans to implement dither control on this rig. The rig consists of two wheels pressed against each other with a defined preload. The upper wheel represents the rail, while the lower wheel represents the wheel. The lower wheel is driven by an electric motor. Different contact positions, angles of attack, normal loads and lateral creepages can be chosen by altering the setup. For both wheels, FE models were created to obtain the wheel receptances in vertical and lateral directions as well as for the coupled direction. In the following the text always refers to a rail although it actually is a rail-disc.

The aim of the design of the rig was to maximise the likelihood of the occurrence of squealing. In simulations it was shown that the modes (2,0,a) in the wheel and in the rail are capable to build up squeal due to mode coupling. The index 2 indicates that there are two wavelengths fitting to the circumference, 0 indicates that there are zero nodal lines in radial direction and  $a$  notes that the modal pattern has its main component in axial direction. Details to the rig can be found in Ref. [42]. A first experimental evaluation of the rig showed that squeal occurred as planned under the condition that contact geometry and creepage were chosen in an appropriate way.

Fig. 3 shows the cross-section of wheel and rail. The nodes where contact was assumed to take place, as well as the position where later on a dither force is applied, are indicated. In addition, the modes (2,0,a) are presented. Table 1 shows the radius of the wheel rail and the rail disc together with the modal damping ratio  $\zeta_n$  as function of the circumferential mode order  $n$ .

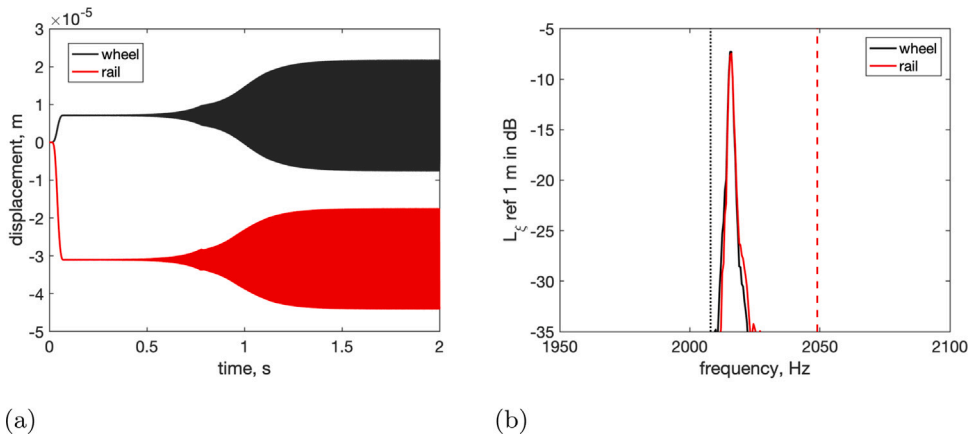


Fig. 4. Building up process of the lateral displacement  $\xi$  of wheel and rail under squeal conditions (a) and the main spectral component of the steady state part of the vibrations (b). The vertical solid line indicates the eigenfrequency for mode (2,0,a) of the wheel (blue) and the dashed vertical line indicates the eigenfrequency for mode (2,0,a) of the rail. (For interpretation of the references to colour in this figure legend, the reader is referred to the web version of this article.)

The results presented in this paper always refer to this contact geometry. Further relevant input data are rolling speed (50 km/h), load (20 kN), and a rigid slip of 0.3 m/s corresponding to a lateral creepage of 2.16%. Coulomb friction was applied with a friction coefficient  $\mu_0$  of 0.55. The surface roughness was set to zero. These parameters were kept for all simulations if not explicitly stated differently.

For the realisation of the dither an additional lateral and/or vertical force is added at the point indicated by the red circle in Fig. 3. Dither forces have also been applied to the rail but did not show significantly different results in comparison with those for the wheel excitation and are therefore not presented in the further text.

#### 4. Self-excitation of curve squeal

Simulations in WERAN are used to demonstrate the generation of friction-induced vibrations for the chosen contact position and a rigid slip value of 0.3 m/s. Fig. 4(a) shows as a typical result the build-up process of the vibrations for the wheel and the rail at the contact point.

Under an initial phase (0.07 s), the pre-load of 20 kN is successively applied by pressing the wheel on the rail. At the same time the creepage is increased from zero to its final value. Inspecting the resulting lateral and vertical displacement, a in the beginning, almost exponential growth can be observed, which starts to slow down from about 0.8 s. At around 1.2 s, the process goes into a saturation phase, in which the system converges to a steady-state condition. The process appears to be governed by the coupling of the modes (2,0,a) in wheel and rail, exchanging energy through the contact, which results in a squeal frequency of about  $f_{squeal} = 2014$  Hz. This lies in between the eigenfrequencies of both (2,0,a) modes as shown in Fig. 4 (right), where the autospectrum of the time signal in the steady-state phase (i.e.,  $t > 1.2$  s) is presented together with indicators for the eigenfrequencies of the both participating modes. When excluding the mode (2,0,a) of the wheel or the rail from the modal summation (see also Section 4.2) describing the dynamic systems, instability is no longer observed in the simulations.

##### 4.1. Explanation of the process behind the self-excited vibrations

The underlying structure of the simulation in WERAN can be presented as a block diagram, as shown in Fig. 5. The blocks  $H_1$  to  $H_4$  describe the combined receptances of wheel and rail for lateral and vertical excitation. The system consists of two main feedback loops, one for the lateral contact and one for the vertical contact.

Both loops have as input static quantities in the form of the rigid slip and the static displacement. Both loops are coupled due to two reasons. Firstly, due to the geometry of the rail and the wheel and the position of the contact, vertical and lateral directions are coupled. This means that a vertical contact force yields a vertical and lateral displacement in the contact position. In the same way as a lateral force also creates a vertical and lateral displacement. Secondly, the vertical force  $F_z(t)$  is directly influencing the lateral force as the friction force  $F_y(t)$  is the product of the momentary friction coefficient  $\mu(\Delta u(t))$  and the vertical force  $F_z(t)$ . The quantity  $\Delta u(t)$  is the relative velocity between rail and wheel in the contact point.

To investigate the importance of the different coupling paths  $H_1$  to  $H_4$  for the occurrence of self-excited vibrations, WERAN has been modified successively by “switching off” combinations of these blocks and re-running the simulations. From these runs one can conclude that block  $H_2$  and block  $H_4$  were not relevant for the self-excitation process. Even if these blocks were “switched off” the self-excited vibrations did develop as before with minor deviations in the amplitudes of the dynamic quantities. Consequently,

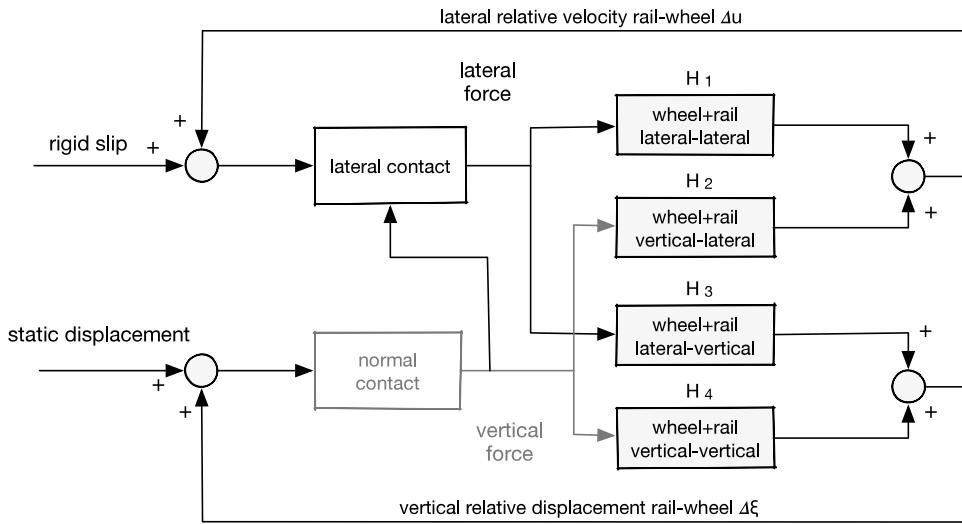


Fig. 5. Block diagram of the complete dynamic system modelled by WERAN.

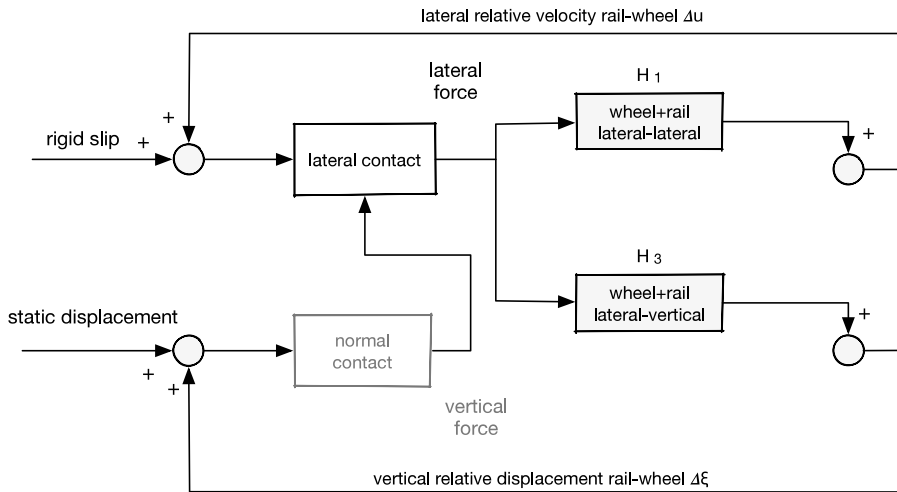


Fig. 6. Block diagram of the dynamic system relevant for the self-excited vibrations.

for the discussion of the mechanisms behind the self-excitation process, it is sufficient to consider the reduced system as shown in Fig. 6.

When “switching off”  $H_3$ , the system is stable and no self-excitation takes place. When “switching off”  $H_1$ , the system is still unstable, but the vibration amplitudes and the resulting forces change substantially. Based on this, we find the feedback loop consisting of the lateral contact,  $H_3$  and the vertical contact. This final loop is shown in Fig. 7, displaying the typical block diagram of a recursive filter. The frequency response  $H_{tot}$  of such a filter can be expressed as

$$H_{tot} = \frac{H_3}{1 - H_3 H_C} \tag{1}$$

In this case, the assumption of a linearised contact has been made. This means that the friction coefficient is assumed to be independent of the difference  $\Delta u$  of the lateral velocity of wheel and rail and corresponds to  $\mu_0$ . In addition the vertical force is linearised assuming that the vertical force  $F_z$  is the contact stiffness  $K_c$  multiplied with the displacement difference  $\Delta \xi$  for wheel and rail. The linearised contact is represented by the transfer function  $H_C = \mu_0 K_c$ .

The stability of such a recursive filter can be investigated by means of the Nyquist stability criterion when plotting the open-loop transfer function  $H_3 H_C$  in the complex plane. Instability occurs where the plot encircles the point  $(1 + j0)$ . At this frequency, the amplification by  $H_3 H_C$  is larger than unity and the phase shift is zero. As shown in Fig. 8, there are a number of frequencies where instability can occur (indicated by dots). For better identification of those frequencies, 8(b) shows just the real part of the open-loop transfer function over frequency. Among those frequencies there also is a frequency close to 2000 Hz, i.e. the eigenfrequency



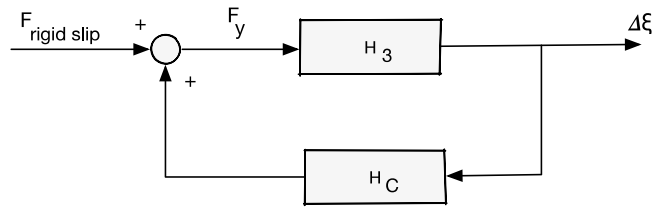


Fig. 7. Blockdiagram of the recursive filter built by the cross receptances of wheel and rail and the linearised vertical and lateral contact formulation.

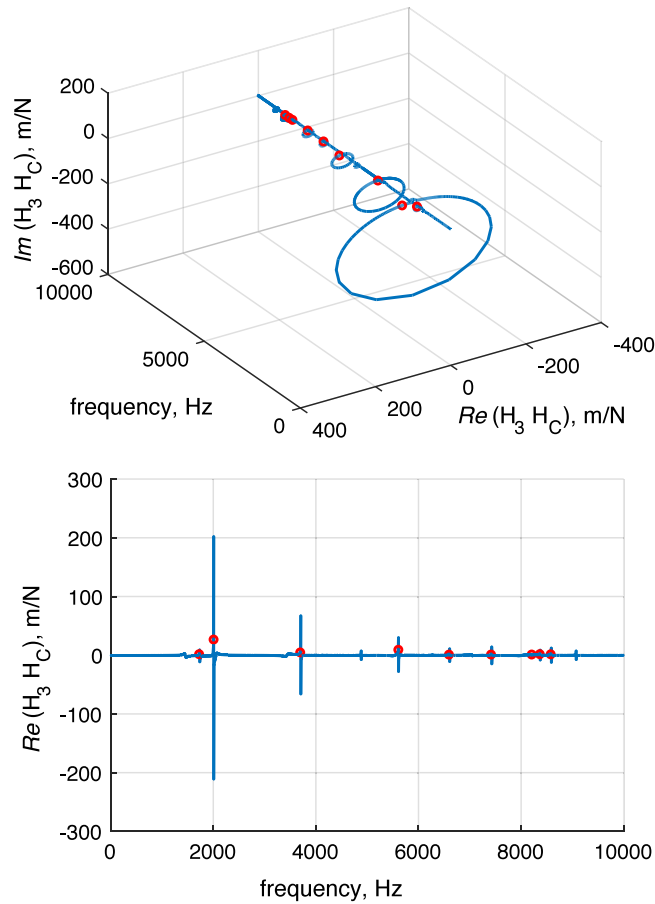


Fig. 8. Nyquist plot of the open-loop transferfunction  $H_3 H_C$  with  $K = 8 \times 10^9$  N/m and  $\mu_0 = 0.55$ . The dots indicate the frequencies where  $Im(H_3 H_C) = 0$  and  $Re(H_3 H_C) > 1$ .

of the modes (2,0,a). When removing these modes from the modal sum for the calculations of the receptances, the open-loop transferfunction  $H_3 H_C$  will not any longer encircle the point  $(1 + j0)$  at this frequency.

Instabilities at other eigenfrequencies have not been found in the simulation of self-excited vibrations in the complete system. However, to fulfil the Nyquist criterion is necessary but not sufficient for the instability of the complete system.

The result also implies that in the case considered here, mode coupling is not necessarily needed to observe instability. As long as the dynamic properties of the components are such that the open-loop transfer function  $H_3 H_C$  delivers zero phase and amplification larger than unity, the system could be unstable. This has also been reported in [9], where it is shown that even in the case of an infinite rail with mass or damping-like behaviour, curve squeal can occur, i.e. in the absence of mode coupling. There it is also stated that the cross-terms of the rail receptances play a minor role for the instability, while here, the mechanism of self-excited vibrations is solely explained by the cross-terms for rail and wheel receptances. However, both cases might not be directly comparable.

Based on the previously described findings, the feedback loop leading to self-excited vibrations can be described as follows.

- **start condition:** At the beginning of the simulations, the wheel is pressed on the rail until the prescribed vertical load is reached. In addition, a rigid slip is applied, which leads to a lateral force. Without a coupling between lateral and vertical



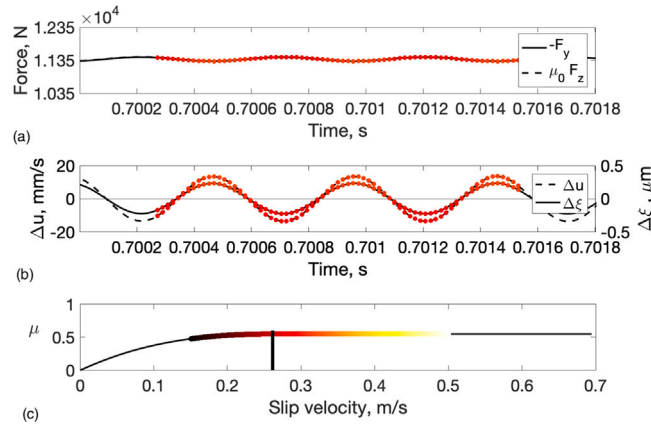


Fig. 9. Description of the dynamic system at the time  $t = 0.7$  during build-up. (a) Lateral and vertical force, (b)  $\Delta u$  and  $\Delta \xi$ , (c) friction curve. (For interpretation of the references to colour in this figure legend, the reader is referred to the web version of this article.)

direction and/or a falling friction curve, this would be a stable situation. However, in the case considered here, the modes (2,0,a) in wheel and rail provide this strong coupling.

- **step1: altering the vertical force:** The coupling between lateral and vertical direction leads to a vertical displacement due to the initially created lateral force. The change in vertical displacement also means a change in the vertical contact force.
- **step2: altering the lateral force:** By changing the vertical force the lateral force is altered (it is the product of the vertical force and the friction coefficient at the working point determined by rigid slip and lateral relative motion).
- **building up process:** The loop between **step1** and **step2** leads to a growing process until the system goes into a saturation condition.
- **saturation:** When the lateral velocity is sufficiently big, the velocity difference between wheel and rail in combination with the rigid slip will be sufficient to reach sticking. Consequently, the lateral force will be reduced as the global friction coefficient will be smaller than for sliding. This limits the growing process as the duration of stick would increase with increasing lateral amplitude  $\Delta u$ .

To illustrate this process, the lateral and vertical forces and the difference ( $\Delta u$ ) of the lateral velocity of wheel and rail and the difference of the vertical displacement ( $\Delta \xi$ ) of wheel and rail are presented in Figs. 9 and 10 during build-up and when saturation is reached. In addition, the information about the momentary working point on the friction curve  $\mu$  is given.

In the initial state (Fig. 9) only sliding can be observed. The oscillations  $\Delta u$  and  $\Delta \xi$  are in phase but very small in amplitude. Therefore sticking is not observed yet. (a) shows the lateral force and the vertical force multiplied with the friction coefficient  $\mu_0$ . In (b) both  $\Delta u$  and  $\Delta \xi$  are presented. The colours in both plots indicate the position of the momentary working point on the friction curve (c). The black vertical line in the plot of the friction curve indicates the transition from purely sliding (right side of the curve) to partial sticking (left side of the curve).

With further development of the self-excited vibrations, the lateral velocity is growing until it is sufficiently big to reach the friction curve left of the indicator between sliding and partly sticking (see Fig. 10). As a consequence, the lateral force is at those time instances reduced and the process goes with further increase of the lateral velocity into a state of saturation.

#### 4.2. Power balance for the self-excited vibrations

Besides discussing the feedback loop, it is also essential to observe the net power flow in the system. For this, the power input and the dissipated power have to be calculated. As wheel and rail are described by a superposition of modes, the calculations are best done for each mode individually. The different steps to reach such a formulation are shown in the following. The starting point is the modal summation

$$v(\mathbf{x}, \omega) = \sum_n v_n(\omega) \Phi_n(\mathbf{x}) \tag{2}$$

where  $v(\mathbf{x})$  is the velocity at a certain position of the wheel or the rail.  $\Phi_n(\mathbf{x})$  are the mode shapes and  $v_n(\omega)$  the modal amplitudes. Assuming a point force  $F_e(\omega)$  at the position  $\mathbf{x}_0$  these are calculated as

$$v_n(\omega) = a_n(\omega) F_e(\omega) \Phi_n(\mathbf{x}_0) \tag{3}$$

with

$$a_n(\omega) = j\omega \frac{1}{\Lambda_n(\omega_n^2 - \omega^2 + j2\omega\omega_n\zeta_n)}. \tag{4}$$

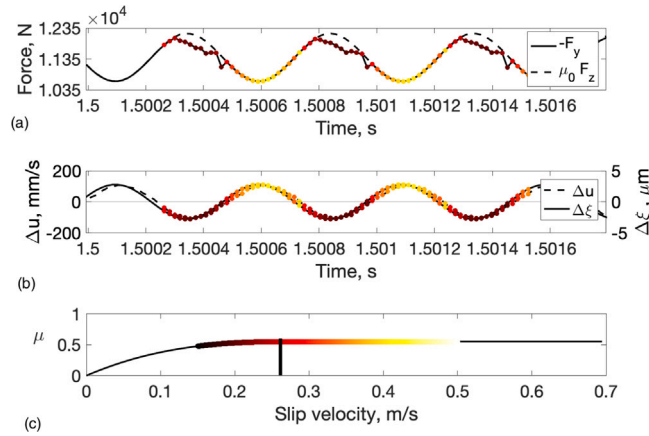


Fig. 10. Description of the dynamic system at the time  $t = 1.5$  s (saturation). (a) Lateral and vertical force, (b)  $\Delta u$  and  $\Delta \xi$ , (c) friction curve.

In this  $\omega_n$  are the eigenfrequencies and  $\omega$  the angular frequency.  $\zeta_n$  is the damping ratio for mode  $n$ . The modal forces  $F_n$  are obtained by expansion of the force distribution in modal components.  $A_n$  is calculated as the integral over the whole volume of the body in the form

$$A_n = \int_0^V m(\mathbf{x}) \Phi_n^2(\mathbf{x}) d\mathbf{x} \tag{5}$$

where  $m(\mathbf{x})$  is the mass density at position  $\mathbf{x}$ . Based on this description it is straightforward to calculate the net power input into a system at position  $\mathbf{x}_0$ . The power input  $W_{in,n}$  for each mode is

$$W_{in,n}(\omega) = 0.5 \Re \{ F_e(\mathbf{x}_0, \omega) v_n^*(\omega) \Phi_n(\mathbf{x}_0) \}. \tag{6}$$

where  $*$  is the conjugate complex. For calculating the dissipated power the reversible (potential) energy  $E_{pot}$  stored in each mode is needed, which yields

$$E_{pot,n} = 0.5 |v_n|^2(\omega) \frac{\omega_n^2}{\omega^2} A_n. \tag{7}$$

The dissipated power for each mode is proportional to the stored reversible energy in each mode

$$W_{loss,n} = \zeta_n \omega_n |v_n|^2(\omega) A_n. \tag{8}$$

In the further discussion, we are interested in the input power and dissipated power as a function of time for each mode, but also for the total system. Due to orthogonality, the total input power and dissipated power is the sum of the power obtained for each mode. The time-domain formulation can be obtained by starting with the Green's function  $g_n(t)$  as the inverse Fourier transform of the driving point mobility. This leads to the expressions

$$W_{in,n}(t, \mathbf{x}_0) = F_e(t) [F_e(t) * g_n(t) \Phi_n(\mathbf{x}_0)] \tag{9}$$

for the input power and

$$W_{loss,n}(t) = g_n(t) g_n(t) A_n \zeta_n \omega_n \tag{10}$$

for the dissipated power. The operator “ $*$ ” indicates the convolution.

These two expressions give the power variation over time. However, for the power balance, we are interested in having the net power flow, i.e. the time average over the power. To obtain this netto power flow from (9) and (10) a moving average is taken over a sufficiently long time period. In the case here, the average is performed over 0.07 s which corresponds to about 140 periods at the squealing frequency around 2000 Hz. In addition the lateral and vertical forces are high-pass filtered to contain only frequency components above 500 Hz to increase the readability of the time series. Otherwise it would have been necessary to increase the time window of the moving average, which also would mean losing time resolution in the results. Fig. 11 shows the results for the case presented previously.

In this case, the lateral power is mainly fed to the rail and dissipated there. The rail has substantially higher damping than the wheel. There is also a small lateral power input to the wheel.

After the initial phase, it seems that all power input into the wheel is coming from the rail in the form of vertical power input. The lateral power input into the wheel ceases out when the self-excitation process goes into the state of saturation, and the rail loses vertical power through the contact corresponding to the power input into the wheel. In the steady-state cycle, the overall power input for rail and wheel converges to the dissipated power in the system based on the damping distribution.

The results underline the coupling between lateral and vertical motion. In steady state condition, only the rail receives lateral power from the contact while the wheel only receives vertical power through the rail. There is no lateral power input into the wheel.

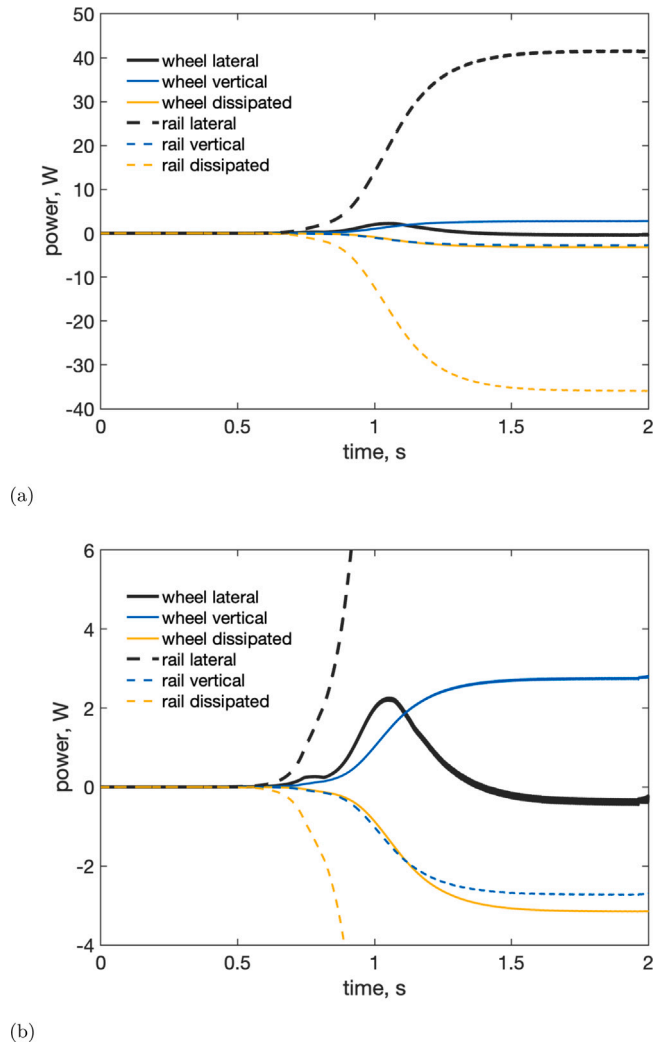


Fig. 11. (a) Net power flow into wheel and rail and due to dissipative losses in wheel and rail. (b) Same picture as in (a) but with different power scale.

### 5. The influence of dither signals

The application of dither means to apply an additional force at the wheel or the rail to influence the processes in the contact. It is done in an open-loop control system, i.e. without synchronising the dither signal with the vibration to be controlled. Such an approach has been previously investigated in [16] for curve squeal in the case of a falling friction curve. For the falling friction curve the feedback loop is solely based on the lateral contact as the change in lateral relative velocity leads to a change in lateral force. This interaction leads to instability. A coupling between lateral and vertical contact forces is not needed in this case.

It might not mean that the function of dither will differ in comparison to the case considered here. However, in [16] very little is said about the physics behind the functioning of the dither. This section, therefore, has the goal to explain the mechanisms behind the functioning of dither to suppress self-excitation. For this, a working hypothesis is presented (Section 5.1). The results from a parameter study are used to validate this hypothesis in Section 5.2. Finally, the potential of dither for the mitigation of curve squeal is discussed.

#### 5.1. Working hypothesis

As the self-excitation process is based on the coupling between frictional forces and vertical displacement, dither has to “destroy” this process. It is assumed that for achieving this, the lateral amplitude due to dither has to be strong enough to reach stick condition in the contact. As long as the wheel and the rail are only sliding on each other, the dither signal and the self-excited vibrations can coexist without any problems. Not until the lateral motion due to the dither is sufficient to create partial stick, the dither can start

to dominate the timing of the process in the lateral contact. The stick–slip motion has to follow the dither frequency. Consequently, the process behind the self-excited vibrations will get weakened or even destroyed.

This description of the functioning of the dither is the working hypothesis in the subsequent text and is investigated in more detail.

### 5.2. Summary of the results from a parameter study

An initial parameter study showed that the dither force can be an arbitrary time signal as long as its frequency content is above the squealing frequency (as also stated in literature for simple friction oscillators). If  $f_{dither}$  (i.e. the dither frequency) is lower than  $f_{squeal}$  (i.e. where squeal occurs without control), the self-excited process could still take place during a stick–slip cycle due to dither.

With respect to the required control effort, it turned out to be the most efficient to use harmonic force signals preferable close to eigenfrequencies of modes not participating in the generation of squeal. By this, sufficiently high lateral amplitudes in the contact between wheel and rail can be created by smaller dither forces. The study also showed that there is no general difference in exciting wheel or rail despite that exciting the wheel is more efficient to excite the wheel due to its higher receptance. Therefore, a more elaborated parameter study is carried out with a lateral harmonic force close to the eigenfrequency of the mode (3,0,a) of the wheel ( $f_{dither} = 3705$  Hz) applied at the side of the wheel (see Fig. 3). The parameter study showed that two main cases can be distinguished.

Case 1: Applying the dither force in advance or during the build-up process of friction induced vibrations when the self-excited vibrations are still small. Fig. 12(a) exemplifies typical results. After switching on the dither force at 0.75 s, squealing continues at a reduced level depending on the amplitude of the dither force.

Case 2: Applying the dither force when the friction-induced vibrations are fully established. In those cases the control effort turned out to be higher. Consequently the efficiency of the approach is reduced as the vibration levels at least on the wheel are due to the dither forces. Fig. 13(a) shows that the squeal frequency is stopped when applying a sufficiently high force. For smaller dither forces, only minor reductions are observed, if any at all.

Both cases can be explained based on the working hypothesis from the previous section. The dither force is now applied from the very beginning. Figs. 14 and 15 show the response of the dynamic system to the harmonic dither force with an amplitude of 150 N and 300 N evaluated at 0.8 s.

From Fig. 14, it is visible that a dither force of 150 N is strong enough to impose a lateral velocity reaching the stick region (indicated by the darker dots for the lateral forces). If the self-excited vibration has not developed strong enough to reach stick, the dither is “dictating” the timing of the stick–slip motion. Consequently self-excited vibrations cannot develop further but will be weakened or even die out. With smaller dither forces, this effect cannot be achieved. This also limits the application of dither to severe cases as independent of the amplitude of the squeal noise, a minimum dither amplitude is always needed, and the noise due to the dither signal might then be stronger than the eventual squeal noise.

If the self-excited vibrations already have developed to their full state, as in case 2, a dither force is needed, which creates a lateral amplitude  $\Delta u$  exceeding the amplitudes due to the self-excited process. Only then, the dither will be able to take over the stick–slip cycle. In the case here, for the amplitude of 300 N, a velocity  $\Delta u$  is achieved which is comparable with the amplitudes in fully developed self-excited vibrations as shown in Fig. 10.

If these amplitudes are achieved, the self-excitation process behind squeal generation collapses. It also means that once the self-excited vibrations have stopped, a small dither amplitude of about 150 N will be sufficient to prevent the build-up of a new squealing event as demonstrated later in the text.

### 5.3. Power balance in the presence of dither

The power balance in Fig. 16 underlines the working hypothesis further. The dither force is switched on at 0.75 s.

For 150 N (b), the power balance can be interpreted as follows. In the first 50 milliseconds after the start of the dither signal, the vibration at  $f_{dither}$  is built up until  $\Delta u$  is sufficient to reach the stick region on the friction curve. At the same time, the power input into the wheel and the rail through the contact is changing. The power input into the rail more or less disappears. So does the lateral power input into the wheel. The power created by the dither force is partly dissipated due to damping in the wheel. However, one can show that the main part is dissipated by the friction in the contact. The power input into the rail is stopped as a consequence that the self-excitation process collapses and that the receptance of the rail at  $f_{dither}$  is very low.

For a dither force of 110 N (Fig. 16, (a)) a similar behaviour can be observed in the initial phase. However, as the resulting velocity difference  $\Delta u$  at  $f_{dither}$  is not strong enough, the self-excited vibrations can continue to build up, although delayed. In the end, the vibrations are fully developed, and the power balance corresponds to the one shown in Fig. 11, besides that additional energy is added to the system by the dither. This behaviour also confirms the working hypothesis.

Results for a simulation time of 6 seconds are shown for case 2 in Fig. 17 where the dither is switched on at 1.3 s. The power balance (a) follows the same pattern as in Fig. 16(b). The main difference is that some time is needed to get the self-excited vibrations to collapse completely. A stronger dither force will shorten the required time. However, it will also limit the overall reduction. The kinetic energy on the wheel and rail is calculated with and without dither. Fig. 17(b), shows the kinetic energy on wheel and rail with dither (solid line) and without dither (dashed line). While for the rail, the difference in kinetic energy reaches more than 20 dB, for the wheel, the difference is more moderate. This is not due to limited success in suppressing the squealing, but due to the required relatively high dither force. This becomes clear when presenting the energy in each mode as a moving average over

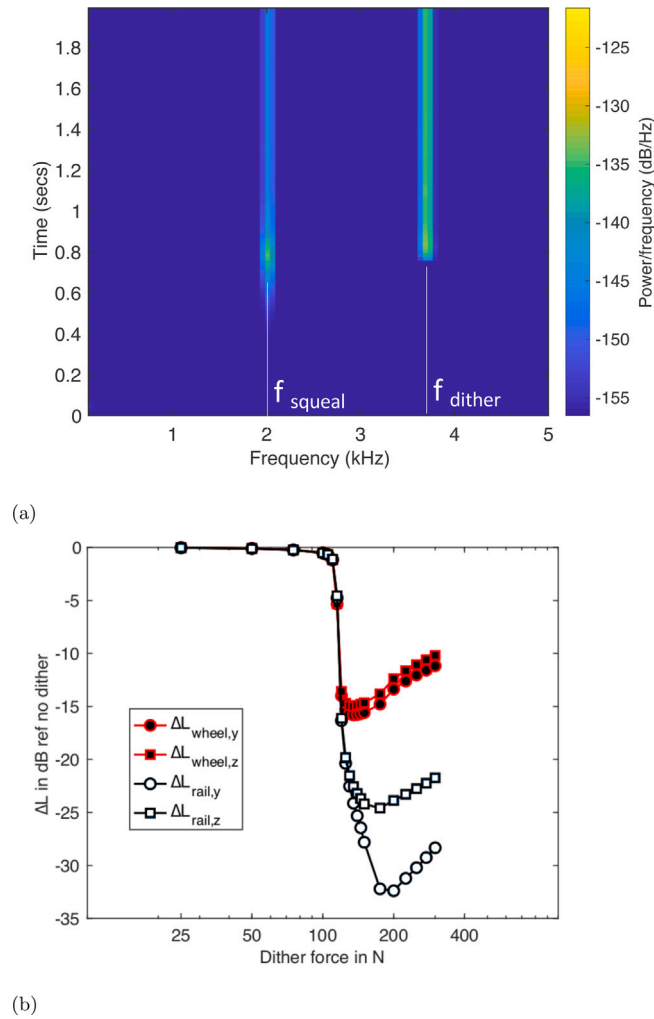


**Fig. 12.** (a) Spectrogram of the lateral wheel displacement with a dither force of 150 N starting at 0.75 s. (b) Reduction of the lateral and vertical displacement levels at the contact position on wheel and rail as function of the dither force. The dither always started at 0.75 s. The reduction is calculated by evaluating the rms value between 1.8 and 2 seconds for the case with dither and the case with no dither.

a time window of 70 ms. At each time instant, the energy of each mode is normalised by the energy in the squealing mode of the wheel when no dither is applied. After switching on the dither signal, the squealing mode (mode number 23 in Fig. 17(c)) rapidly decays. However, the mode excited by the dither signal (mode number 34) now determines the overall energy on the wheel. As the rail has no resonances close to  $f_{dither}$ , the dither signal is not able to add significant energy to the rail.

#### 5.4. Potential of dither to mitigate curve squeal

The overall reduction of the kinetic energy achieved on the wheel is rather moderate in case 2 due to the high dither force required to control the already established self-excited vibrations. However, if the self-excited vibrations have collapsed, one could apply a lower force to prevent the build-up of a new self-excited vibration cycle. This is demonstrated in Fig. 18, where after 2.5 s, the dither force is reduced from 300 N to 150 N. In this case the reduction of the kinetic energy on the wheel clearly exceeds 10 dB. Although the kinetic energy might be a good indicator for the sound radiation from the wheel assuming that all modes have a radiation efficiency close to unity, in the end, one has to optimise the application of dither with respect to radiated sound. The main question is if it is possible to create a high lateral velocity at the dither frequency while having low sound radiation at this frequency.

### 6. Conclusion

WERAN has been applied to investigate the mechanisms behind self-excited vibrations leading to curve squeal. It also has been used to study the potential of dither for curve squeal mitigation. The time-domain simulations were applied to a setup of the

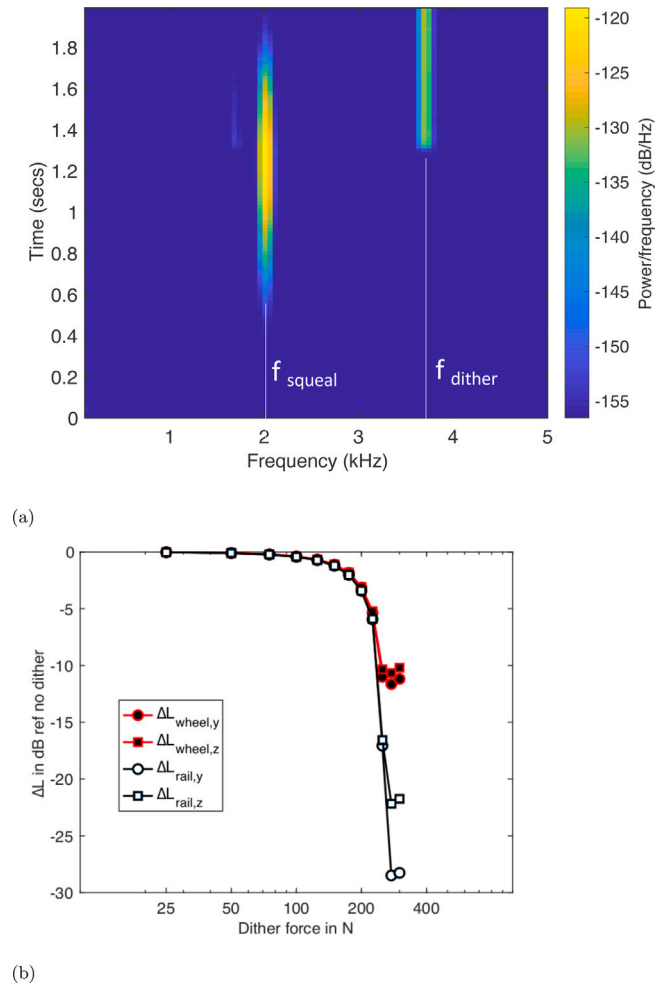


Fig. 13. (a) Spectrogram of the lateral wheel displacement with a 300 N starting at 1.3 s. (b) Reduction of the lateral and vertical displacement levels at the contact position on wheel and rail as function of the dither force. The dither force always starts at 1.3 s. The reduction is calculated by evaluation the rms value between 1.8 and 2 seconds for the case with dither and the case with no dither.

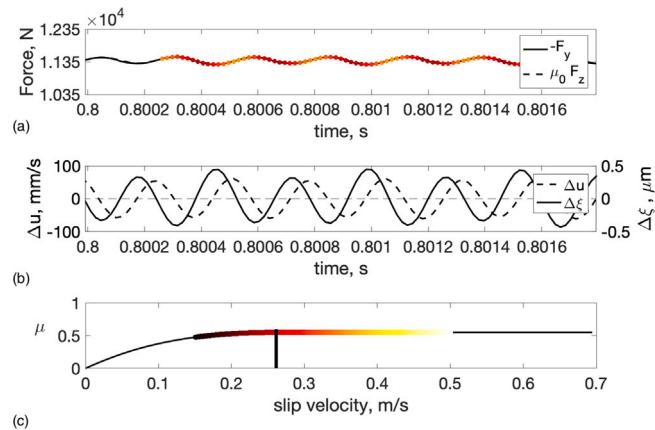


Fig. 14. Response of the dynamic system due to a dither force of 150 N. (a) Lateral and vertical force, (b)  $\Delta u$  and  $\Delta \xi$ , (c) friction curve.

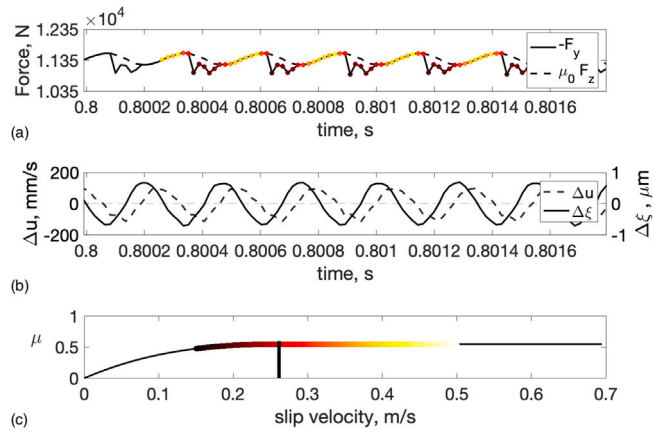


Fig. 15. Response of the dynamic system due to a dither force of 300 N. (a) Lateral and vertical force, (b)  $\Delta u$  and  $\Delta \xi$ , (c) friction curve.

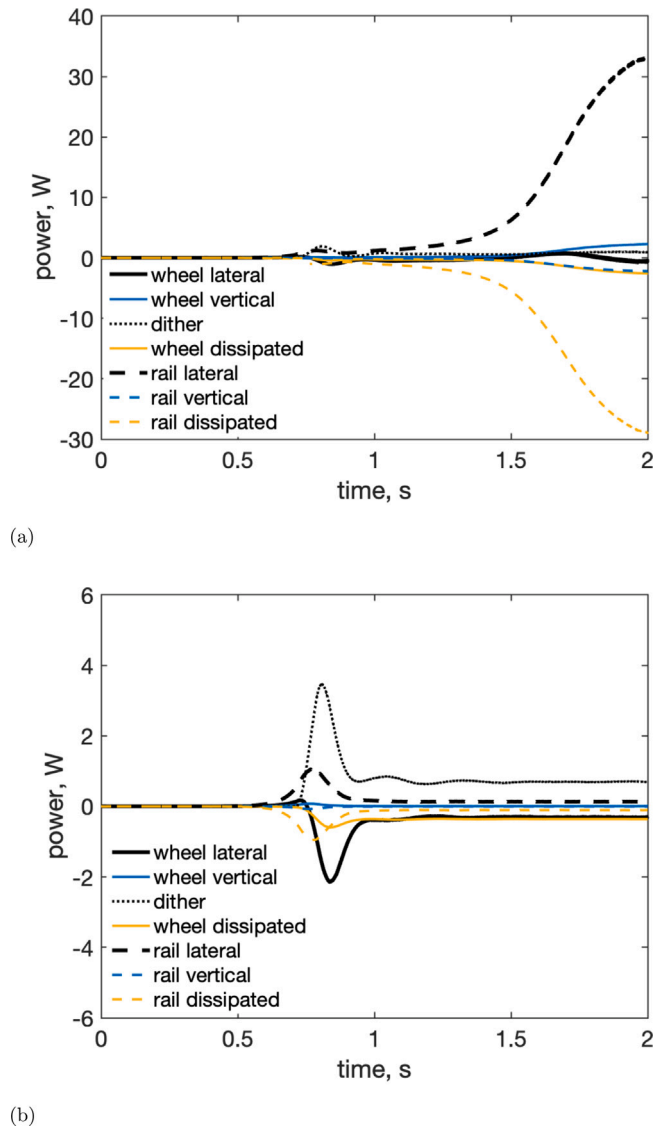


Fig. 16. Net power flow into wheel and rail and due to dissipative losses in wheel and rail for a dither force of 110 N (a) and 150 N (b).



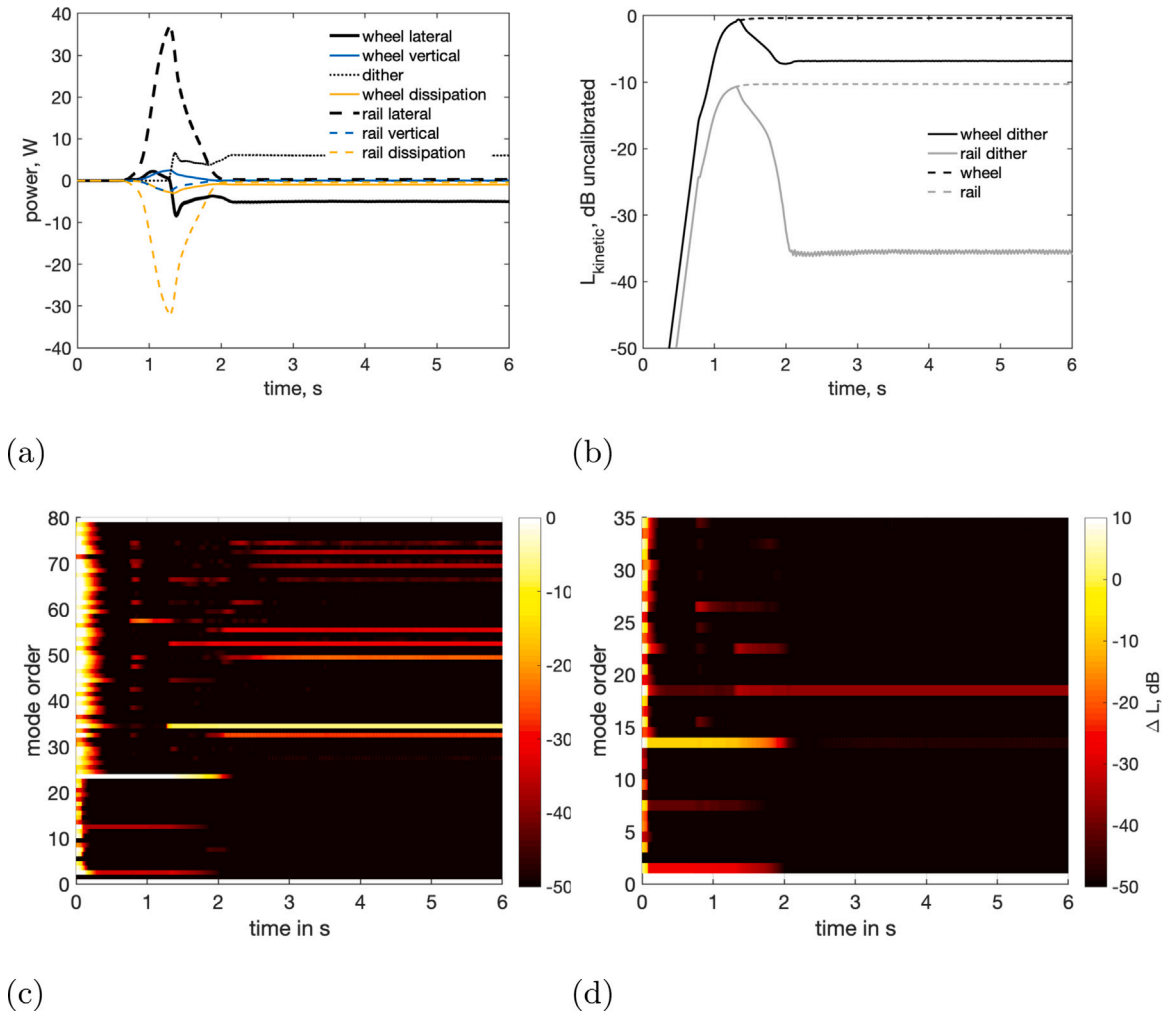


Fig. 17. Results for a dither force of 250 N starting at 1.3 s. (a) Power balance, (b) kinetic energy in wheel and rail with and without dither, (c) normalised kinetic energy in the modes of the wheel and (d) normalised kinetic energy in the modes of the rail.

squealing noise rig at Applied Acoustics, Chalmers University of Technology. Wheel and rail were represented by two flexible wheels. Constant friction was assumed. The analysis of this situation identified the coupling between lateral and vertical direction as the driving mechanism for building up self-excited vibrations. The lateral force leads to a vertical displacement. The change in vertical displacement also means a change in the vertical contact force that then modifies the lateral force. This loop has been shown to be unstable in the sense of the Nyquist stability criterion. The open-loop stability depends on the receptances of wheel and rail as well as on the contact stiffness and the friction curve. The results indicate that, although the presence of modes in wheel and rail is needed, instability can also occur without mode coupling. It might be sufficient with one mode only as long as the coupling between lateral force and vertical displacement is strong enough in the vicinity of the eigenfrequency of this mode.

It is shown that the application of dither is able to hinder the build-up process of self-excited vibrations or to disturb already built-up vibrations to a degree that they collapse. The main condition for this is that the lateral amplitude due to the dither force is strong enough to reach partial stick condition in the contact. As long as wheel and rail are only sliding on each other, the dither signal and the self-excited vibrations can coexist without problems. Not until the lateral motion due to the dither is sufficient to create partial stick, the dither can start to dominate the timing of the process in the lateral contact. Consequently, the stick-slip motion has to follow the dither frequency and the process behind the self-excited vibrations will get weakened or even destroyed. The required dither force is higher if self-excited vibrations are already established than if the vibrations are only in the build-up phase and have not reached the stick-slip cycle yet. However, after a larger force has managed to get fully developed self-excited vibrations to collapse, the force can be reduced to a lower level which is sufficient to prevent the build-up of a new self-excited vibration cycle.

To make the approach suitable for practical implementation demands technical solutions for sufficiently strong excitation of the wheel or the rail. This also decides whether the approach really would open for fast and cheap retrofitting both on track and wheel.

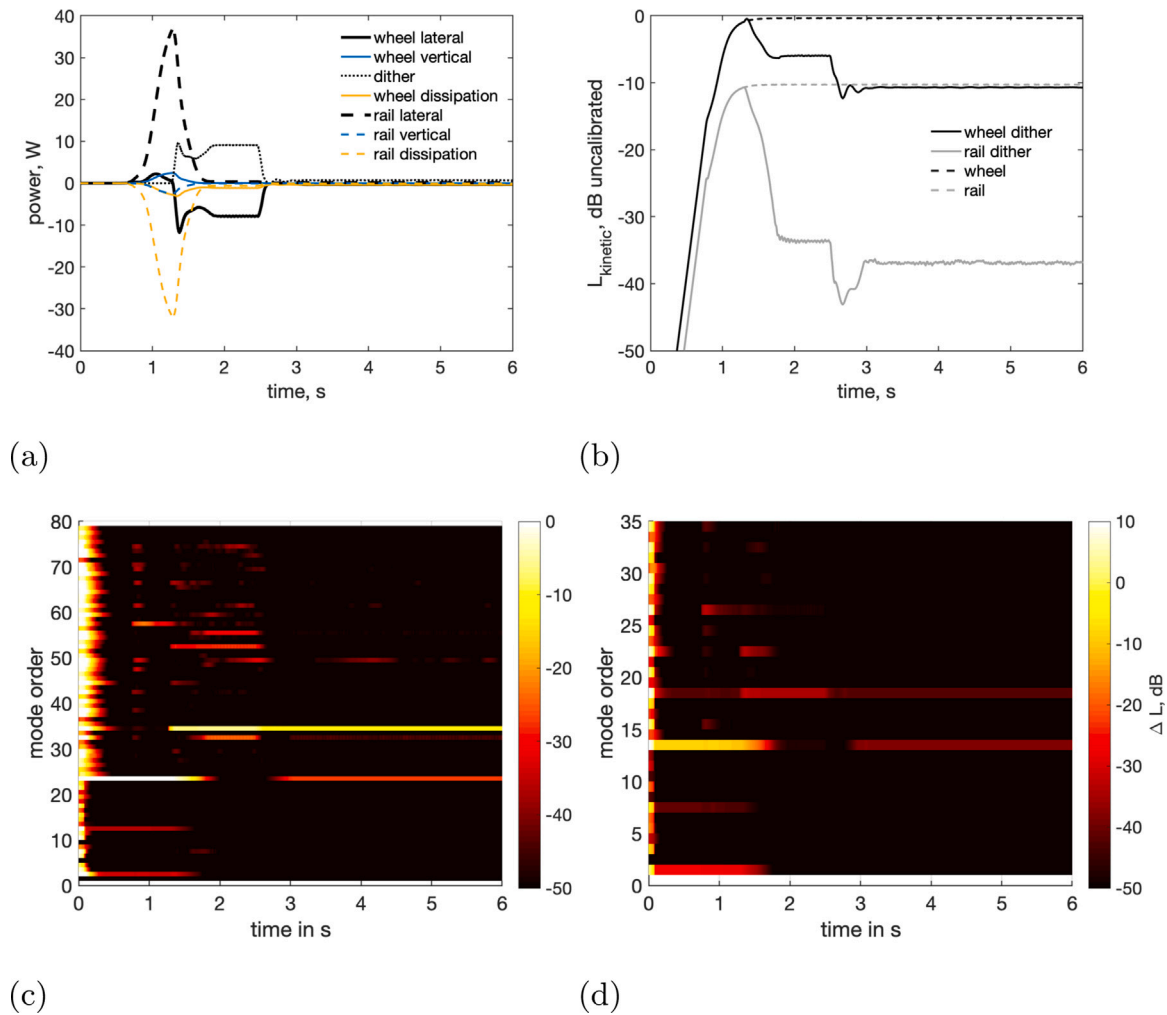


Fig. 18. Results for a dither force of 300 N starting at 1.3 s which at 2.5 s is reduced to 150 N. (a) Power balance, (b) kinetic energy in wheel and rail with and without dither, (c) normalised kinetic energy in the modes of the wheel and (d) normalised kinetic energy in the modes of the rail.

### CRedit authorship contribution statement

**Wolfgang Kropp:** Conceptualization, Methodology, Software, Investigation, Writing - original draft, Writing - review & editing. **Jannik Theysen:** Software, Investigation, Writing - review & editing. **Astrid Pieringer:** Software, Investigation, Writing - review & editing.

### Declaration of competing interest

The authors declare that they have no known competing financial interests or personal relationships that could have appeared to influence the work reported in this paper.

### Acknowledgements

The current study is part of the ongoing activities in CHARMEC - Chalmers Railway Mechanics ([www.chalmers.se/charmec](http://www.chalmers.se/charmec)). Parts of the study have been funded from the European Union's Horizon 2020 research and innovation programme in the project In2Track2 under grant agreement No 826255.

### References

- [1] R. Müller, J. Oertli, Combating curve squeal: monitoring existing application, *J. Sound Vib.* 293 (2006) 728–734.

- [2] D.J. Thompson, *Railway Noise and Vibration: Mechanisms, Modelling and Means of Control*, Elsevier, Oxford, UK, 2009.
- [3] M.J. Rudd, Wheel/rail noise - part II: Wheel squeal, *J. Sound Vib.* 46 (3) (1976) 381–394.
- [4] F.G. de Beer, M.H.A. Janssens, P.P. Kooijman, Squeal noise of rail-bound vehicles influenced by lateral contact position, *J. Sound Vib.* 267 (2003) 497–507.
- [5] P.J. Remington, Wheel/rail squeal and impact noise: What do we know? What do not we know? Where do we go from here? *J. Sound Vib.* 116 (2) (1985) 339–353.
- [6] J.T. Oden, J.A.C. Martins, Models and computational methods for dynamic friction phenomena, *Comput. Methods Appl. Mech. Engrg.* 52 (1985) 527–634.
- [7] N. Hoffmann, M. Fischer, R. Allgaier, L. Gaul, A minimal model for studying properties of the mode-coupling type instability in friction induced oscillations, *Mech. Res. Commun.* 29 (2002) 197–205.
- [8] Ch. Glocker, E. Cataldi-Spinola, R.I. Leine, Curve squealing of trains: Measurement, modelling and simulation, *J. Sound Vib.* 324 (2009) 365–386.
- [9] B. Ding, G. Squicciarini, D.J. Thompson, Effect of rail dynamics on curve squeal under constant friction conditions, *J. Sound Vib.* 442 (2019) 183–199.
- [10] V.-V. Lai, O. Chiello, J.-F. Brunel, P. Dufrénoy, The critical effect of rail vertical phase response in railway curve squeal generation, *Int. J. Mech. Sci.* 167 (2020) 1052881.
- [11] B. Dirks, P.K. Wiersma, Asymmetric rail profile to prevent railway squeal noise, in: Paper presented at the Turkish Acoustical Society - 36th International Congress and Exhibition on Noise Control Engineering, INTER-NOISE 2007 ISTANBUL, Vol. 1, 2007, pp. 72–80.
- [12] D.T. Eadie, M. Santoro, W. Powell, Local control of noise and vibration with KELTRAC friction modifier and protector trackside application: An integrated solution, *J. Sound Vib.* 267 (3) (2003) 761–772.
- [13] D. Anderson, N. Wheatley, Mitigation of wheel squeal and flanging noise on the Australian rail network, *Notes Numer. Fluid Mech. Multidiscip. Des.* 99 (2008) 399–405.
- [14] J.B. Müller, E. Jansen, F.G. de Beer, Curve Squeal WP3 Toolbox of Existing Measures, Report Prepared by SBB and TNO, Union Internationale des Chemins de Fer, 2013.
- [15] J.F. Brunel, P. Dufrénoy, J. Charley, F. Demilly, Attenuation of the squeal noise of railway wheels using metallic rings, in: Paper presented at the Tenth International Congress on Sound and Vibration, 2003, p. 1681–1688.
- [16] S.R. Marjani, D. Younesian, Application of dithering control for the railway wheel squealing noise mitigation, *Smart Struct. Syst.* 23 (4) (2019) 347–357.
- [17] M.A. Heckl, Active control of the noise from a Rijke tube, *J. Sound Vib.* 124 (1) (1988) 117–133.
- [18] J.R. Seume, N. Vortmeyer, W. Krause, J. Hermann, C. Hantschk, P. Zangl, A. Orthmann, Application of active combustion instability control to a heavy duty gas turbine, *J. Eng. Gas Turbines Power* 120 (4) (1998) 721–726.
- [19] M. Chen, C.R. Knospe, Control approaches to the suppression of machining chatter using active magnetic bearings, *IEEE Trans. Control Syst. Technol.* 15 (2) (2007) 220–232.
- [20] J.D. Jansen, L. van den Steen, Active damping of self-excited torsional vibrations in oil well drill strings, *J. Sound Vib.* 179 (4) (1995) 647–668.
- [21] M.A. Heckl, I.D. Abrahams, Curve squeal of train wheels, part 1: Mathematical model for its generation, *J. Sound Vib.* 229 (3) (2000) 669–693.
- [22] M.A. Heckl, Curve squeal of train wheels, part 2: Which wheel modes are prone to squeal? *J. Sound Vib.* 229 (3) (2000) 695–707.
- [23] M.A. Heckl, X.Y. Huang, Curve squeal of train wheels, part 3: Active control, *J. Sound Vib.* 229 (3) (2000) 709–735.
- [24] J. Vanderkooy, S.P. Lipshitz, Resolution below the least significant bit in digital systems with dither, *J. Audio Eng. Soc.* 32 (3) (1984) 106–113.
- [25] M.F. Wagdy, Effect of various dither forms on quantization errors of ideal A/D converters, *IEEE Trans. Instrum. Meas.* 38 (4) (1989) 850.
- [26] O. Morgül, On the control of some chaotic systems by using dither, *Phys. Lett. A* 262 (1999) 144–151.
- [27] F.C. Moon, A. Reddy, W.T. Holmes, Experiments in control and anti-control of chaos in a dry friction oscillator, *J. Vib. Control* 9 (3–4) (2003) 387–397.
- [28] M.A. Michaux, A.A. Ferri, K.A. Cunefare, Effect of tangential dither signal on friction induced oscillations in an SDOF model, *J. Comput. Nonlinear Dyn.* 2 (3) (2007) 201–210.
- [29] K.A. Cunefare, Experimental active control of automotive disc brake rotor squeal using dither, *J. Sound Vib.* 250 (4) (2002) 579–590.
- [30] J. Bardetscher, K.A. Cunefare, A.A. Ferri, Braking impact of normal dither, *J. Vib. Acoust.* 129 / 17 (2007).
- [31] M.A. Michaux, A.A. Ferri, K.A. Cunefare, Effect of waveform on the effectiveness of tangential dither forces to cancel friction-induced oscillations, *J. Sound Vib.* 311 (3–5) (2008) 802–823.
- [32] U. Fingberg, A model for wheel-rail squealing noise, *J. Sound Vib.* 143 (1990) 365–377.
- [33] F.J. Périard, *Wheel-Rail Noise Generation: Curve Squealing by Trams* (Ph.D. thesis), TU Delft, 1998.
- [34] Z.Y. Huang, D.J. Thompson, C.J.C. Jones, Squeal prediction for a boogied vehicle in a curve, in: B. Schulte-Werning, et al. (Eds.), *Noise and Vibration Mitigation for Rail Transportation Systems*, in: NNFM 99, Springer-Verlag, Berlin, Heidelberg, 2008, pp. 313–319.
- [35] J. Giner-Navarro, J. Martínez-Casas, F.D. Denia, L. Baeza, Study of railway curve squeal in the time domain using a high-frequency vehicle/track interaction model, *J. Sound Vib.* 431 (2018) 177–191.
- [36] J. Jiang, I. Ying, D. Hanson, D. Anderson, An investigation of the influence of track dynamics on curve noise, in: *Proceedings IWRN11, Uddevalla*, September 2013.
- [37] J.J. Kalker, A fast algorithm for the simplified theory of rolling contact, *Veh. Syst. Dyn.* 11 (1982) 1–13.
- [38] Pieringer, A numerical investigation of curve squeal in the case of constant wheel/rail friction, *J. Sound Vib.* 333 (18) (2014) 4295–4313.
- [39] J.J. Kalker, *Three-Dimensional Elastic Bodies in Rolling Contact*, Kluwer Academic Publishers, Dordrecht, Boston, London, 1990.
- [40] I. Zenzerovic, A. Pieringer, W. Kropp, Towards an engineering model for curve squeal, *Noise Vib. Mitig. Rail Transp. Syst.* (2014) 433–440.
- [41] I. Zenzerovic, W. Kropp, A. Pieringer, An engineering time-domain model for curve squeal: Tangential point-contact model and Green's functions approach, *J. Sound Vib.* 376 (2016) 149–165.
- [42] A. Aglat, J. Theyssen, Design of a Test Rig for Railway Curve Squealing Noise (Master thesis BOMX02-17-86), Department of Civil and Environmental Engineering, Division of Applied Acoustics, Chalmers University of Technology, 2017.